Growth and magnetic anisotropy of Fe films deposited on Si(111) using an ultrathin iron silicide template

G. Garreau,* S. Hajjar, J. L. Bubendorff, and C. Pirri
Laboratoire de Physique et de Spectroscopie Electronique, 4 rue des frères Lumière - 68093 Mulhouse, France

D. Berling, A. Mehdaoui, R. Stephan, P. Wetzel, S. Zabrocki, and G. Gewinner
Laboratoire de Physique et de Spectroscopie Electronique, 4 rue des frères Lumière - 68093 Mulhouse, France

S. Boukari and E. Beaurepaire
Institut de Physique et de Chimie des Matériaux de Strasbourg, 23 rue du Loess - 67034 Strasbourg, France
(Received 7 October 2004; published 30 March 2005)

The growth and magnetic properties of thin Fe films deposited at room temperature on ultrathin iron silicide seed layer epitaxially grown on Si(111) single crystal were investigated as a function of Fe thickness ($0 < t_{Fe} < 300$ monolayers). The growth mode and structure have been determined *in situ* by means of scanning tunneling microscopy, low energy electron diffraction, and x-ray photoelectron diffraction. The magnetic properties were characterized *ex situ* by conventional polar and longitudinal magneto-optical Kerr effect, transverse biased initial inverse susceptibility and torque (TBIIST) measurements, and superconducting quantum interference device magnetometry. Fe growth is of Volmer-Weber type (island growth) and the epitaxial film adopts the bcc α-Fe structure. Onset of long-range ferromagnetic order occurs at 4.7 monolayers (ML), in the vicinity of the percolation threshold of the Fe islands. The Curie temperature increases continuously with Fe coverage, varying from 135 K for 4.7 ML to 260 K for 7.3 ML. Two different spin reorientation transitions have been observed versus Fe coverage. First, the magnetic easy axis rotates from normal to the film plane, for coverage below 6 ML, to in plane, for thickness above 7 ML. Then, in-plane magnetized films present tiny (anisotropy fields less than 4 Oe) uniaxial and sixfold magnetic anisotropies. From sixfold anisotropy the small higher order cubic anisotropy constant K_2 was measured precisely by TBIIST. It decreases monotonously with increasing coverage and changes its sign at approximately 20 ML, which in turn results in a switching of the sixfold anisotropy easy axis from $\langle 1\text{–}10 \rangle$ to $\langle 1\text{–}21 \rangle$ directions. It appears that TIBIIST magnetometry is a powerful method for a quantitative determination of the various contributions to in-plane magnetic anisotropies in ultrathin films.

DOI: 10.1103/PhysRevB.71.094430 PACS number(s): 75.30.Gw, 68.35.Bs, 75.70.Ak, 78.20.Ls

I. INTRODUCTION

During the past two decades, a great number of studies have been devoted to the growth and magnetic properties of thin ferromagnetic transition metals on semiconductors. Quite a few of them concerned the systems Fe/GaAs (Refs. 1–9) and Fe/ZnSe.[10–12] It has been shown that it is possible in both systems to obtain epitaxial Fe layers with a strong uniaxial in-plane magnetic anisotropy, and without interdiffusion at the Fe/semiconductor interface. The integration of magnetic layers in Si-based devices has motivated recent studies concerning Fe films grown directly on Si wafer.[13–21] Unfortunately, a strong intermixing occurs at the Fe/Si interface even at room temperature.[14,17,18] The thickness, structure, and stoichiometry of the interface Fe-Si alloy depend critically on the preparation conditions (substrate temperature, substrate orientation, deposition rate, iron thickness…) and are not controlled. At any rate, Si diffusion in Fe can result in the formation of undesirable so-called "magnetic dead layers." To avoid this strong and uncontrolled Fe/Si chemical reaction, several approaches have been proposed. Growth of epitaxial Fe layers without interdiffusion succeeded on Si substrate by inserting thin buffer layers such as metallic Cu,[22–24] semiconducting GaSe,[25] or insulating CaF_2.[26,27] The insertion of ultrathin deposit of Au, which acts as a surfactant, reduces significantly the Fe/Si intermixing.[28] The passivation of the Si surface with Sb is another method proposed in the literature to suppress the uncontrolled silicide formation at the Fe/Si interface.[29] Alternatively, a well-controlled epitaxial silicide seed layer can be intentionally formed to limit Si migration from the substrate and promote Fe epitaxy, as it has been previously demonstrated for the $Fe/FeSi_2/Si(001)$ system.[30]

Recent results showed that high quality epitaxial iron silicide with $c(4\times8)$ periodicity can be obtained by solid phase epitaxy on Si(111) substrate.[31,32] As the surface of this silicide is homogeneous, atomically flat and thermally stable up to 850–900 K, this ultrathin silicide could be an interesting template for the integration of Fe films on Si(111).

In the present article, we investigate first the growth (morphology and structure) at room temperature (RT) of thin Fe films deposited at normal incidence on this $c(4\times8)$ iron silicide seed layer. We focus then on the magnetic properties (onset of ferromagnetism and magnetic anisotropy) of these Fe films. In particular, we show that two spin reorientation transitions (SRT) occur as a function of Fe thickness (t_{Fe}). The first one corresponds to a rotation of the magnetic easy direction from the film normal (for $t_{Fe} < 6$ monolayers) to-

ward in the film plane (for $t_{Fe} > 7$ monolayers), as usually observed in the case of thin Fe (Refs. 16, 22, and 33–37) and Co (Refs. 38–40) layers. The second one is specific to the (111) orientation of the Fe films and has never been observed previously, to our knowledge. It is associated with a reorientation of the sixfold in-plane cubic magnetic easy axis at approximately 20 monolayers, as evidenced by highly sensitive transverse biased initial inverse susceptibility and torque (TBIIST) measurements.

II. EXPERIMENT

The substrate was *B*-doped Si(111) wafer ($\rho \sim 0.2\ \Omega$ cm). After a short rinse in ethanol, the substrate was inserted into the ultrahigh vacuum (UHV) chamber. The substrate was degassed by direct heating up to 900 K for 10 h and flashed afterwards at 1450 K to remove the native oxide layer. After repeated flashes at 1450 K for increasing durations (up to one minute), the substrate was cooled rapidly to 1200 K and then slowly (at a rate of 1 K/s) down to RT. A sharp 7×7 pattern was observed by low energy electron diffraction (LEED). Scanning tunneling microscopy (STM) showed terraces larger than 100 nm and a defect-free 7×7 atomic structure. The ultrathin ($\sim$8 Å) iron silicide template was formed by solid phase epitaxy: 1.7 monolayer (ML) Fe (one monolayer is defined as the atomic density of a Si(111) plane, i.e., 7.8×10^{14} atom/cm^2) is deposited at RT and the sample is postannealed for 20 min at $\sim$850 K. The template covers homogeneously the Si substrate and is atomically flat, as previously described in Ref. 31. The Fe films were grown at normal incidence by keeping the substrate at RT. The deposition rate determined by a water-cooled quartz crystal microbalance was fixed to about 0.3 ML per minute. The nominal Fe thickness (t_{Fe}) is given with a precision better than 10%. The sample preparation as well as the LEED, STM, and x-ray photoelectron diffraction (XPD) measurements were performed in three connected UHV chambers with a base pressure below 1×10^{-10} mbar. After completion of the LEED, STM, and XPD analysis, the sample was covered at RT by a 50-Å-thick Ge layer and removed from UHV for the magnetic characterization. XPD measurements were carried out using a hemispherical analyzer operating at an angular resolution of ±1°. XPD scans were obtained by measuring the intensity of the Fe $2p_{3/2}$ core level doublet (kinetic energy of 779 eV) excited with an Al K_α x-ray source ($h\nu = 1486.6$ eV). The LEED patterns were collected at normal incidence with a four-grid optics. STM measurements were performed with a commercial RT-operating microscope (STM-AFM Omicron). The STM tungsten tips were electrochemically etched and cleaned *in situ* by *e*-beam heating. The STM images were collected in the constant-current mode. The magnetic properties were investigated *ex situ* by means of two distinct magneto-optical Kerr effect (MOKE) polarimeters and a superconducting quantum interference device (SQUID) magnetometer. With the first MOKE magnetometer, magnetization loops were collected from 77 to 400 K both in polar and longitudinal geometries. In order to determine accurately the different tiny contributions of the magnetic in-plane anisotropy, we performed TBIIST measurements with a RT-operating MOKE setup. The recently developed TBIIST method is described in detail in Ref. 41. For both MOKE magnetometers, the incidence angle of the laser beam ($\lambda = 633$ nm) is about 45° with respect to the sample normal.

III. FILM MORPHOLOGY AND STRUCTURE

The evolution of the surface morphology versus Fe thickness is depicted in Fig. 1. The first image [Fig. 1(a)] corresponds to the atomically flat template layer. As shown in detail in Refs. 31,32, its topmost atomic layer consists of a $p(2\times2)$ Si adatom (each protrusion in the inset is a Si adatom) network, whereas the periodicity in subsurface is $c(4\times8)$. Large $c(4\times8)$ domains—rotated with respect to each other by 120°—are clearly visible on the STM image and reflect in the LEED pattern of Fig. 3(a). After deposition of 1 ML [Figs. 1(b) and 1(c)], four types of domains (labeled A, B, C, and D) are present. A domains are covered by atomic protrusions forming locally small $p(2\times2)$ networks. These protrusions are Si adatoms from the initial template layer. At this stage, a significant part of the original bare template surface is left unchanged. *B* domains consist of depressions (darkest grey level) whose lateral extension is typically below 1 nm^2. These depressions are missing Si adatoms. In contrast C and D domains present no atomic resolution. C domains (brightest gray level) consist of randomly distributed small clusters containing typically less than 5 atoms. These clusters are most likely Fe islands. They cover less than 20% of the sample surface for a nominal Fe thickness of 1 ML. It indicates that substantial part of the incident Fe atoms reacted with Si atoms from the two topmost Si layers of the seed layer to form an Fe-Si alloy. This intermixed phase forms D domains (second darkest gray level). At a coverage of 2 ML [Fig. 1(d)], $p(2\times2)$ Si adatom networks are no more visible, i.e., the initial Si adatom layer was entirely consumed to form Fe-Si alloy areas D domains). The size and density of Fe clusters increase in comparison with 1 ML coverage, but they are still well separated by D domains. The islands have essentially the same thickness that, unfortunately, could not be determined accurately from STM since the basal plane and the islands have different chemical composition. Nevertheless, if we neglect these spectroscopic effects and assume that the Fe islands are Si free, the volume of the islands can be estimated, by multiplying their height and area. We found that this volume involves less than half the deposited Fe amount, the remainder is in the reacted Fe-Si areas (confirming the substantial Fe-Si reaction that leads to the formation of an iron silicide sea around the Fe islands). The Fe islands start to coalesce around 3.5 ML, forming meanders on the whole surface [Fig. 1(e)]. Some sparse thicker islands (brightest gray level) start to form. For coverage higher than 5 ML, all Fe islands are connected and entirely cover the surface [Figs. 1(f)–1(i)]. Consequently, the morphological percolation of the islands occurs in the 4–5 ML thickness range. The island size (lateral extension and height) continuously increases with the thickness as shown in Fig. 2, where both rms roughness and island mean diameter are reported versus Fe coverage. Actu-

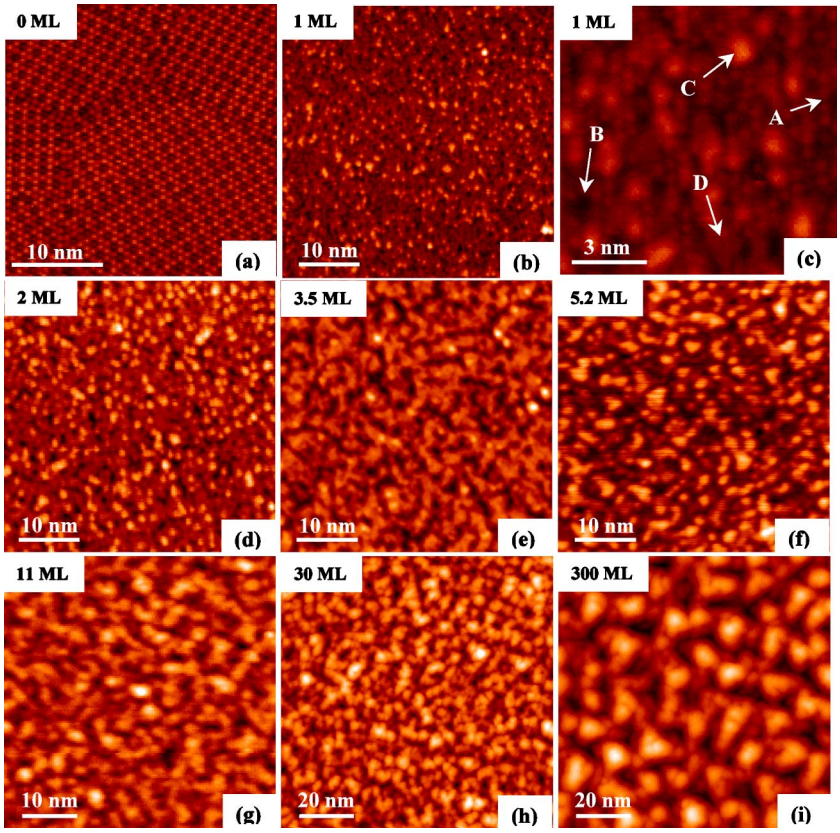

FIG. 1. A series of STM images showing the evolution of the surface morphology of RT-deposited Fe(111) films as a function of Fe coverage (0–300 ML). All the images are taken at a positive sample bias of 2 V and a tunneling current of 0.1 nA. Note that the surface area changes from 45×45 nm^2 [(a),(b),(d)–(g)] to 100×100 nm^2 [(h),(i)]. The image (c) is an atomically resolved zoom collected for 1 ML coverage.

ally these parameters plotted versus film thickness show basically simple power laws as expected from general scaling theory considerations on film growth.[42] Such an island growth mode (Volmer-Weber growth mode) was expected. Indeed, the surface diffusion of Fe atoms at RT is such as the Schwoebel barriers are effective and suppress the step-down diffusion of impinging Fe atoms, leading to the formation of islands.[43] A more detailed analysis[42] of the STM images for thick Fe films ($t_{\mathrm{Fe}}>300$ ML) showed that the majority of the Fe islands have a pyramidlike shape with approximately a threefold symmetry and expose (110) and equivalent facets.

Fe epitaxy is evidenced by LEED experiments as shown in Fig. 3. A LEED pattern is visible at any rate in the 0–300 ML Fe deposit range. At the first stage of the growth ($t_{\mathrm{Fe}}\leqslant4$ ML), the spots are sharp and intense [Figs. 3(b) and

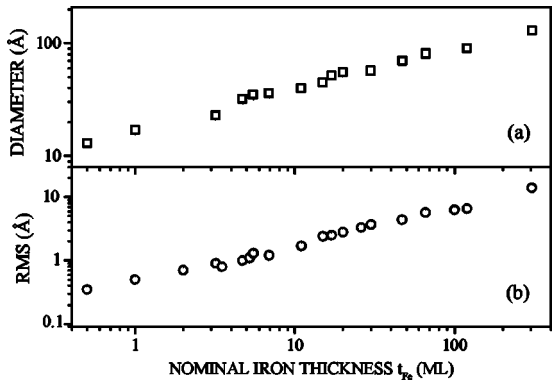

FIG. 2. Island mean diameter (a) and rms roughness (b) versus Fe coverage.

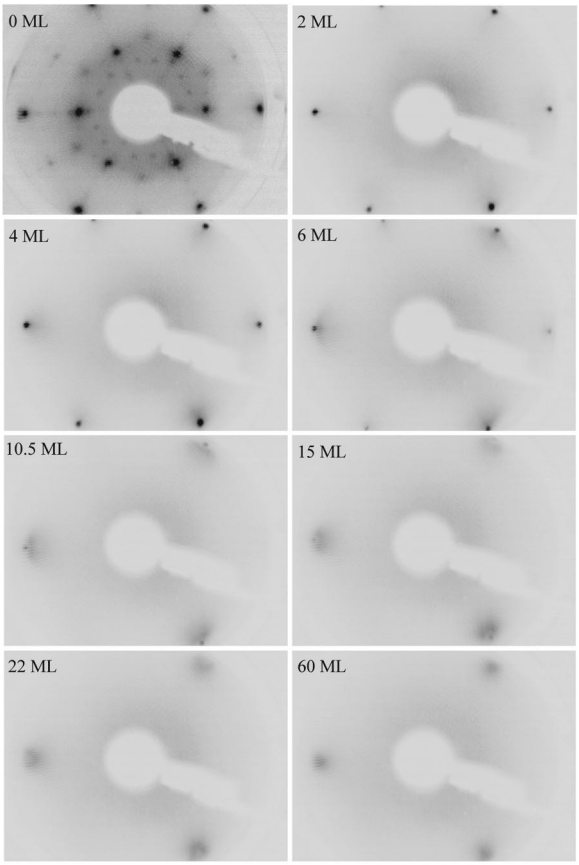

FIG. 3. LEED patterns at 34 eV versus Fe coverage. The LEED intensities have been inverted black to white.

3(c)]. From 5 to 15 ML, their intensity decreases drastically whereas their sharpness does not change. Additional large and diffuse spots appear progressively, superimposed to the sharp spots. For coverage above 20 ML, only the large and faint diffraction spots are visible [Figs. 3(g) and 3(h)]. These large spots become gradually narrower and more intense upon increasing the thickness.

The evolution of the LEED pattern versus Fe coverage is in line with the previous STM analysis. Indeed, the initial sharp and intense spots [Figs. 3(b) and 3(c)] are relevant to the large iron silicide area (domains D). This silicide that forms coherently on the initial seed layer adopts most likely the cubic CsCl-$FeSi_x$ ($0<x<2$) structure. The drop of the sharp spots intensity between 4 and 6 ML results from the morphological percolation of the Fe islands. These Fe islands sign as the diffuse spots in the LEED pattern. At a coverage above the morphological percolation threshold $t_{Fe}>5$ ML, the large diffuse spots arise from the 3D Fe islands that cover the whole surface. The weak intensity and large width of these spots clearly indicate that Fe islands are smaller than the coherence length of our LEED equipment (and rough). The continuous decrease of the spot width upon increasing the thickness above 20 MLs results from the increase of the mean island size. That is, the lateral extension of coherent scattering area inside a given island increases progressively, but remains smaller than the coherence length of the diffracted low-energy electrons, which is estimated to about 10 nm. This is in agreement with the fact that the island mean diameter gradually increases with the thickness, but remains below 10 nm (for the thickest film). Finally, the continuous decrease of the sharp spots intensity for increasing coverage between 6 and 15 ML results from the gradual attenuation of the iron silicide signal by the growing Fe islands (the inelastic electron mean free path being less than 7 Å at 34 eV).

The structure of the epitaxial Fe films and its orientations with respect to the substrate were determined by means of XPD. Figure 4 shows XPD polar scans measured for different nominal Fe thickness. The scans were taken in the Fe(110) plane from the [111] surface normal ($\theta=0°$) toward the $[1\text{-}21]_{\text{Si substrate}}$ direction ($\theta=90°$). XPD polar scans calculated using double scattering codes[44] for equivalent thickness are also reported in Fig. 4. In these simulations, Fe is assumed to crystallize in its bulk bcc structure with Fe(111)∥Si(111) and the cluster radius around the emitter atom was set to 12 Å. The marked modulations of the experimental scans indicate that the Fe film is well ordered, in agreement with the previous LEED analysis. The simulations reproduce fairly well the experimental spectra, whatever the film thickness.[45] In particular, the small structure around 15° is nicely visible on both the simulated and experimental curves only for coverage higher than 10 ML. Moreover, the intense forward-focusing peaks are located at the same polar angles ($\theta=0°$, 30°, and 55°) for both Fe film and template. These results clearly show that Fe adopts the bcc structure and the epitaxial relationships between the Fe layer, the iron silicide template and the Si substrate are the following: Fe(111)∥$c(4\times8)$(111)∥Si(111) and Fe[-12-1]∥$c(4\times8)$[-12-1]∥Si[1-21]. Note that similar structural orientations have been obtained previously using $p(2\times2)$ iron silicide as seed layer.[41]

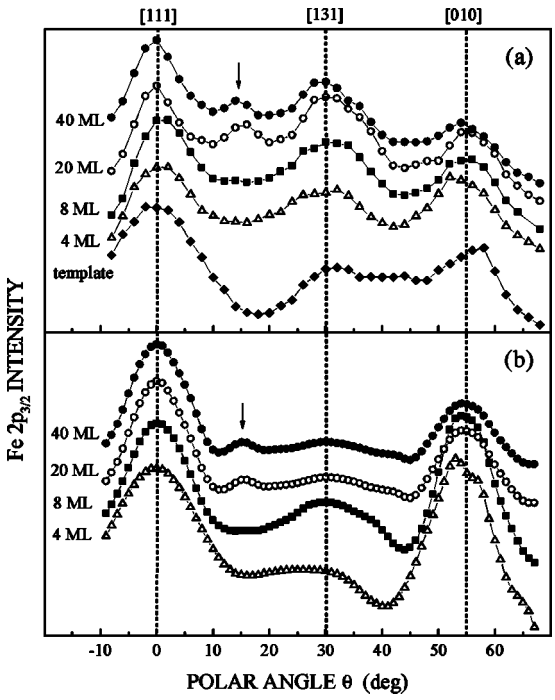

FIG. 4. Experimental (a) and simulated (b) XPD polar scans of the Fe_{2p} core line in the (110) plane from the [111] surface normal ($\theta=0°$) toward the $[1\text{-}21]_{\text{Si substrate}}$ direction ($\theta=90°$) as a function of Fe coverage. The three major peaks at $\theta=0°$, 30°, and 55° correspond to the internuclear axes [111], [131], and [010], respectively. Note that the small peak at about $\theta=15°$ appears for both simulated and experimental scans for coverage above 10 ML.

IV. MAGNETIC PROPERTIES

A. Out-of-plane toward in-plane spin reorientation transition

To investigate the presence of ferromagnetic order and the magnetic anisotropy in the Fe films, we collected Kerr magnetization loops both in polar and longitudinal geometries[46] between 77 and 300 K. For the thinnest layers ($t_{Fe}<5$ ML) SQUID measurements have also been performed from 10 to 300 K with the external magnetic field applied either in the film plane, or perpendicularly to the film plane. In the whole 10–300 K temperature range, no ferromagnetic response (i.e., hysteresis loop) was detected for nominal thickness below 4.5 ML. For coverage above 4.5 ML, all films are ferromagnetic at 77 K. Kerr hysteresis loops collected for 4.7, 5.7, 6.3, 7.3, and 11 ML films at various temperatures are shown in Fig. 5. Both polar and longitudinal loops of the two thinnest films (4.7 ML and 5.7 ML) indicate that the magnetic easy direction is normal to the film plane [Figs. 5(a)–5(d)]. Indeed, whereas the polar loop exhibits a nearly square-shaped loop with full remanence, a strong field (>1 kOe) is necessary to rotate the magnetization toward the film plane in the longitudinal geometry. Note that the full remanence also observed in longitudinal geometry results from a small misalignment of the external field with respect to the film plane and from the fact that in vanishing external magnetic field, the magnetization lies perpendicular to the film surface, i.e., the Kerr signal corresponds to the out-of-plane magnetization component (mixing of polar and longi-

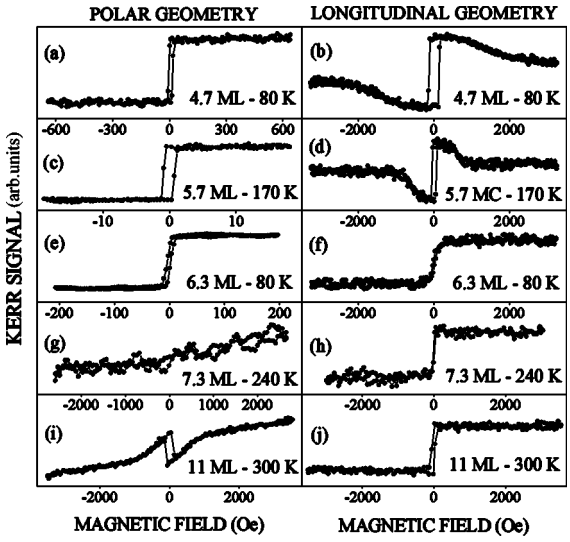

FIG. 5. Magnetization Kerr loops collected in polar (left panel) and longitudinal (right panel) geometries at various temperatures for different Fe coverage: 4.7 ML–80 K (a),(b), 5.7 ML–170 K (c),(d), 6.3 ML–80 K (e),(f), 7.3 ML–240 K (g),(h), and 11 ML–300 K (i),(j).

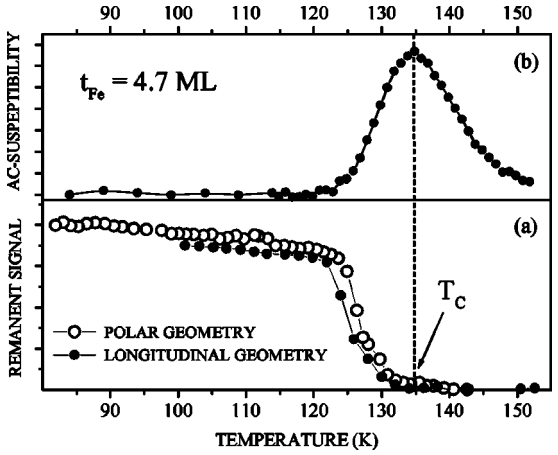

FIG. 6. Remnant Kerr signals (a) and real part of the magnetic susceptibility (b) versus temperature, for 4.7-ML-thick Fe film. Kerr signals were recorded in polar (open circles) and longitudinal (full circles) geometries. The susceptibility was measured by SQUID with a small ac field (amplitude: 3.5 Oe; frequency: 20 Hz) applied along the film normal.

tudinal Kerr effects). At coverage of 6.3 ML, the remnant magnetization is less than 20% of the saturation magnetization in both polar and longitudinal geometries. Moreover, a rather small external magnetic field (<200 Oe) is sufficient to align the magnetization along the magnetic field direction in both geometries. It indicates that in zero external field either the magnetization is canted if we assume a single domain magnetization, or there is a statistical distribution of in-plane and out-of-plane magnetized domains. For coverage above 7 ML, Kerr loops are typical for in-plane magnetized film [Figs. 5(g)–5(j)]. The hysteresis loop in longitudinal geometry is nearly square and the saturation is reached with a small field, whereas the signal in polar geometry is typical for a hard axis loop with no saturation up to the highest available field (~ 3 kOe). Note that in Fig. 5(i) the hysteresis loop superimposed on the hard axis loop is due to the longitudinal Kerr effect (in-plane magnetization component) and its presence results from both the large incident angle of the laser beam ($\sim 45°$) and a small misalignment of the external magnetic field with the sample normal.

To summarize, the different Kerr loops in Fig. 5 clearly indicate a SRT from out-of-plane toward in-plane with increasing thickness. Such a thickness-driven SRT has already been observed in the case of thin Fe films.[16,22,33–37] As often discussed in the literature, this SRT reflects the competition between the perpendicular uniaxial surface anisotropy and the shape anisotropy. For the thinnest layers ($t_{Fe}<6$ ML), the uniaxial surface or interface anisotropy resulting from the reduced symmetry in the surroundings of the surface atoms is larger than the shape anisotropy and forces the magnetization to lie perpendicular to the film plane. Since the shape anisotropy energy due to the demagnetizing field is a volume effect, it overcompensates the surface anisotropy energy above a critical thickness (~ 7 MC in the present case), thus turning the magnetization in the film plane. As the Fe layer is under compressive strain in the film plane [the lattice mismatch $\eta=(a_{\alpha-\mathrm{Fe}}-a_{\mathrm{template}})/a_{\mathrm{template}}$ is about 5%], a perpendicular rhombohedral distortion that deviates the structure from that of the bcc structure is present for the thin layers. Such a distortion and relevant broken cubic symmetry could also lead to a significant part of the perpendicular uniaxial anisotropy via magnetoelastic effects. Note that this strain and related effect on anisotropy is expected to decrease with increasing Fe film thickness as confirmed by x-ray diffraction.[42] Finally, the XPD analysis showing that the local symmetry around a given Fe versus Fe coverage remains basically cubic, the SRT does not result from some drastic structural modifications, like the martensitic fcc$\rightarrow$bcc transformation, as observed in the case of the Fe/Cu(111) system for instance.[22]

B. Onset of ferromagnetism

The Curie temperature of the Fe films was determined from the thermal variations of the remnant Kerr signal. In Fig. 6(a) the remnant Kerr signal recorded in polar geometry is plotted versus temperature for the 4.7-ML-thick film. The signal vanishes at a critical temperature (~ 135 K) that we define as the Curie temperature (T_C), as it is usually done in the literature. We also reported in Fig. 6(a) the remnant Kerr signal collected in longitudinal geometry to show that this critical temperature is not an out-of-plane toward in-plane reorientation temperature. The phase transition from the ferromagnetic to the paramagnetic state was confirmed by the thermal variations of the magnetic susceptibility measured by SQUID with a small oscillating field. Indeed, the real part of the ac susceptibility presents a maximum at the temperature that corresponds to the disappearance of the remnant Kerr signals [Fig. 6(b)]. The variation of T_C versus nominal Fe thickness is presented in Fig. 7. T_C is considerably reduced in our very thin films compared to the bulk value of α-Fe ($T_C=1143$ K), and T_C increases continuously with the

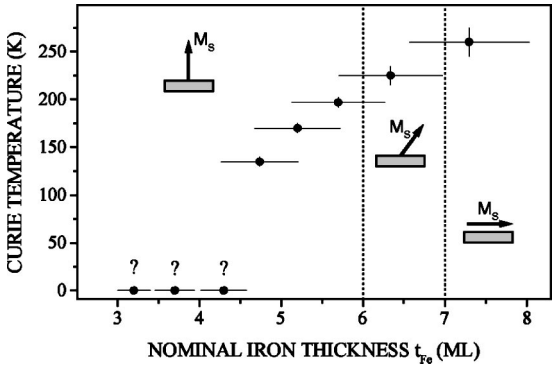

FIG. 7. Variations of the Curie temperature as a function of Fe coverage. For coverage below 4.7 ML (i.e., 3.3 ML, 3.7 ML, and 4.3 ML) no ferromagnetic response could be detected in the whole 10–400 K temperature range (see text).

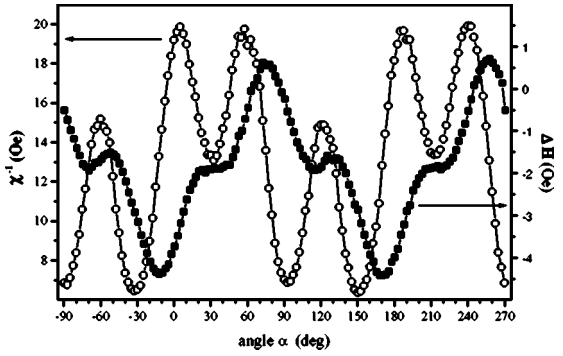

FIG. 8. Torque amplitude ΔH (full squares) and inverse susceptibility χ^{-1} (open circles) versus in-plane angle α for 47-ML-thick Fe film. The transverse bias field H_{per} is 20 Oe. Fourier analysis gives the following twofold and sixfold anisotropy fields: $K_U/M_S = 1.8$ Oe and $K_2/M_S = 0.27$ Oe.

thickness (at a slope of about 60 K/ML). Both features have been observed previously in a lot of ferromagnetic thin films.[8,33,47–54] They result from finite-size[55,56] and spin-spin interaction range[57] effects. In the present case, Fe-Si and Fe-Ge intermixing also contributes. For coverage above 8 ML, T_C is higher than 300 K and, consequently, could not be reached without irreversible change of the as-grown Fe film morphology or structure. As mentioned before, the ferromagnetic response disappears in the whole 10–300 K temperature range for coverage below 4.5 ML. Several reasons may be invoked for the delayed onset of ferromagnetism compared to the case of Fe layers deposited on metallic substrates.[33,51] First, here again there is no doubt that some intermixing between Fe and Si (Fe and Ge) occurs at the Fe or template (Fe or capping layer) interface. Consequently, the thinnest Fe layers contain probably a significant amount of Si and Ge atoms. Previous studies showed that in thick Fe_xSi films the Curie temperature and the amplitude of the Fe magnetic moment decreases drastically with x.[58] For instance, Fe atom loses its magnetic moment at RT for x smaller than 1.35 due to electronic hybridization between $3d$ Fe and $2p$ Si orbitals. In the present case, the absence of ferromagnetic response for coverage below 4.5 ML should therefore correspond to so-called "magnetic dead layers." Another possibility, which is in line with the previous STM analysis and seems therefore well appropriated to explain the delayed onset of ferromagnetic ordering, is a kind of magnetic percolation phenomenon during the coalescence process of the Fe islands, as suggested previously by Bensch[8] in the case of ultrathin Fe layers deposited on GaAs(001) substrate. Indeed, STM images showed that Fe islands start to coalesce at about 3.5 ML and the island percolation threshold is between 4 and 5 ML. At lower coverage, Fe nanoscale-sized islands are disconnected and the film could behave as an assembly of superparamagnetic clusters with a blocking temperature below 10 K. It is also plausible that the dipolar interactions between the disconnected Fe islands are not negligible and lead to a superantiferromagnetic coupling between the islands due to the perpendicular anisotropy, as observed for the Fe/W(110) system.[59] At the morphological percolation threshold the direct exchange coupling between connected Fe clusters leads to magnetic percolation responsible of the sudden long-range ferromagnetic ordering at about 4.7 ML.

C. Rotation of the in-plane cubic sixfold magnetic easy axis

To analyze the thickness dependence of the in-plane magnetic anisotropy for RT in-plane magnetized Fe film ($t_{\text{Fe}} > 8$ ML) we used a recently developed method coined TBIIST. Let us first summarize the principle of this method described in more detail in Ref. 41. The TBIIST for transversely biased initial inverse susceptibility (χ^{-1}) and torque (ΔH) measurements are carried out with a standard MOKE geometry in a longitudinal configuration but under an in-plane static bias field H_{per} applied perpendicular to the longitudinal sweep field H. The data around $M_L = 0$ (M_L is the longitudinal component of the magnetization) are collected and the two quantities χ^{-1} (inverse susceptibility) and ΔH (sweep field offset at $M_L = 0$) are determined. It can be shown that a Fourier analysis of the variations of $\chi^{-1}(\alpha)$ and $\Delta H(\alpha)$ versus the angle α between H_{perp} and a reference direction in the film plane ($[1\text{-}21]_{\text{Fe}}$ in the present case) gives by two independent ways the symmetry, magnitude, and direction of the in-plane magnetic anisotropy contributions.[41] Both $\chi^{-1}(\alpha)$ and $\Delta H(\alpha)$ variations give within experimental error identical results. As an example the variations of χ^{-1} and ΔH versus α for 50 ML Fe are reported in Fig. 8. Each curve presents two contributions reflecting a cubic six-fold symmetry and a twofold symmetry. It indicates that the in-plane magnetic anisotropy is the superposition of a cubic sixfold and an uniaxial contribution. To discuss the magnitude and the easy axis direction of each anisotropy component we have to define first the anisotropy energy of the film. The structural analysis showed that the Fe film adopts the bcc structure and the film plane corresponds to the (111) plane. The first two terms of the magnetocrystalline energy density in this (111) plane can be written as[19]

$$E_{\text{mc}}^{(111)} = \frac{K_1}{4} + \frac{K_2}{108}(1 + \cos 6\alpha), \tag{1}$$

where α is the angle between the magnetization and $\langle 1\text{-}21 \rangle$

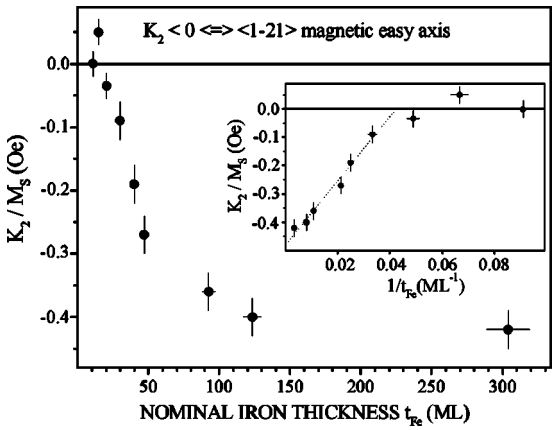

FIG. 9. Thickness dependence of the sixfold magnetic anisotropy fields. Inset: sixfold anisotropy field versus reciprocal film thickness.

direction, and K_1 and K_2 are the first two cubic anisotropy constants. The expression (1) indicates that the cubic magnetocrystalline anisotropy exhibits a sixfold symmetry in the (111) plane and the sixfold anisotropy amplitude is only a result of the higher order by the K_2 term. To describe the additional uniaxial magnetic anisotropy present in our films we may define the total anisotropy energy density by the following expression:

$$E_a = \frac{K_1}{4} + \frac{K_2}{108}(1 + \cos 6\alpha) + K_u \sin^2(\alpha - \alpha_u), \qquad (2)$$

where K_u is the uniaxial magnetic anisotropy constant, and α_u is the angle between the uniaxial magnetic easy axis and the $\langle$1-21$\rangle$ crystallographic direction.

A Fourier analysis of the torque variations $\Delta H(\alpha)$ yields K_2, α_u, and K_u for all RT in-plane magnetized Fe films ($t_{\mathrm{Fe}} > 8$ ML). Actually due to the presence of fourth-order anisotropy K_1 and finite values of in-plane applied fields, the magnetization does not stay exactly in film plane but makes a small angle with it, typically about 0.1°, depending on α. This modifies slightly the measured torque and an effective ${K_2}^{\mathrm{eff}}$ is obtained instead of K_2 that must be corrected according to the relation[60]

$${K_2}^{\mathrm{eff}} = K_2 - \frac{3{K_1}^2}{2\pi {M_S}^2}. \qquad (3)$$

The correction is found to be negligible except above 60 ML coverage. K_1 is obtained approximately from ratio of polar and longitudinal contributions to the Kerr signal. It depends on film thickness in a way fairly similar to the one observed and extensively discussed previously in the case of iron films on Si(001).[61]

The variations of K_2 versus coverage are presented in Fig. 9. K_u and α_u values for various Fe coverage are reported in Table I. Before discussing the different thickness-dependence of K_2, θ_u, and K_u, it is worthwhile to underline the extreme sensitivity of the TBIIST method. This technique is able to separate and determine very accurately different tiny contributions of the in-plane magnetic anisotropy for very thin layers. For instance, anisotropy fields as low as 0.1 Oe can be readily detected.

TABLE I. Uniaxial anisotropy field and orientation α_u of the in-plane uniaxial magnetic anisotropy easy axis with respect to the $[1\text{-}21]_{\mathrm{Fe}}$ crystallographic direction, for different Fe coverage.

t_{Fe} (ML)	11	15	20	30	47	90	120	300
K_u/M_s (Oe)	1.4	1.4	1.5	1.4	1.8	2.8	1.1	4.0
α_u (deg)	5	8	25	40	35	38	20	5

We observe first that, except for the thinnest layer (10 ML), K_2 decreases monotonously with increasing thickness, and changes its sign at approximately 20 ML. The sign of K_2 indicates the magnetic easy direction: a positive (negative) value corresponds to the equivalent $\langle$1-10$\rangle$ ($\langle$1-21$\rangle$) crystallographic directions. The change of sign versus thickness thus indicates that the sixfold magnetic easy axis rotates from the in-plane $\langle$1-10$\rangle$ directions toward the $\langle$1-21$\rangle$ axes. Different reasons could explain the monotonous variations of K_2 with coverage. First, it is common practice in thin film studies to decompose the effective ith-order magnetic anisotropy constant K_i as follows:

$$K_i = K_i^v + \frac{2K_i^s}{t_{\mathrm{Fe}}}, \qquad (4)$$

where K_i^v and K_i^s are the so-called volume and surface or interface terms, respectively. The phenomenological expression (4) has been verified for second- and fourth-order anisotropy constants in the case of several thin epitaxial ferromagnetic films.[39,40,47,62,63] In the present case, K_2 apparently follows the relation (4) on a large thickness range (30 $\rightarrow$300 ML) as it is clearly illustrated by the dotted line in the inset of Fig. 9. Nevertheless, the values of the three thinnest layers clearly deviate from the linear variation. As T_C is much higher than RT for the 15–20 ML coverage range, we can exclude that this significant deviation results from thermal effects (too large reduced temperature T/T_C). On the other hand, it is very likely that the very small K_2 value for the 10-ML-thick film is related to the fact that its Curie temperature is just above RT, as suggested by the $T_C(t_{\mathrm{Fe}})$ variations reported in Fig. 7. Hence this value will not be included in the present discussion since the K_i are expected to depend strongly on the reduced temperature. Nevertheless it appears clear that the thickness dependence of K_2 and the critical thickness t_c around 20 ML cannot be accounted for by a pure surface or interface effect, as described by relation (4). Secondly, the monotonous decrease of the amplitude of K_2 with the reduction of the thickness could be tentatively explained by intermixing between Fe and Si. Indeed, it is well known that Si impurities in Fe reduce significantly the magnetic anisotropy in comparison with pure Fe. For instance, 10% Si in thick Fe layer divides the fourth-order anisotropy constant K_1 by a factor two.[64] Consequently, the continuous increase of the amplitude of K_2 with t_{Fe} could be related to a continuous decrease of the mean Si concentration in the Fe layer. Nevertheless, the K_2 amplitude for t_{Fe}=40 ML is about half

than the value for 300 ML coverage. It would suggest that at least 10% Si is in the 40-ML-thick film, which corresponds to a nominal Si thickness larger than 4 ML. As the homogeneous iron silicide template prevents the diffusion of Si from the substrate toward the Fe film, only the two topmost Si atomic planes (which represent a nominal thickness of 1.25 ML) from the seed layer may react with the Fe film. Moreover, the sign of the magnetic anisotropy constant does not change with the Si concentration in thick Fe-Si film.[64] We must thus conclude that this second explanation plays only a minor role. A third possible effect of Fe thickness change on K_2 is similar to the one we proposed in the case of thin Fe films deposited on Si(001).[61] It was observed that the fourth-order anisotropy constant K_2 increases continuously from 10 to 80 ML and changes sign around 18 ML. We showed that the evolution of this anisotropy versus thickness results mainly from a monotonous decrease of the in-plane compressive biaxial strain in the film with increasing thickness via magnetoelastic effects. Preliminary x-ray diffraction experiments indeed indicate a strong thickness dependence of the in-plane strain in the present Fe films, too.

Let us finally consider the uniaxial component of the in-plane magnetic anisotropy. It appears that the uniaxial anisotropy field is actually a very small effect (less than 4 Oe). The azimuthal orientation of the uniaxial magnetic easy axis relative to the $[1\text{-}21]_{Fe}$ direction fluctuates randomly between 5° and 40° versus Fe thickness. Thus, it seems not related to any peculiar crystallographic axis. Moreover, distinct samples with the same nominal thickness and prepared under identical conditions present different uniaxial directions.[65] This tiny uniaxial anisotropy does not result from symmetry breaking due to the deposition geometry, the incident Fe atomic flux impinging the surface at normal incidence. Indeed, in case of off-normal Fe deposition[66,67] the surface topography consists of long-range iron stripes leading to large uniaxial anisotropies (much stronger than the present one) with magnetic easy axis parallel to the stripes. The origin of the tiny uniaxial anisotropy in our films is not yet clear but may be due to a small vicinality ($<0.1°$) of the nominal (111) surface.

V. SUMMARY

Thin bcc α-Fe films have been epitaxially grown by molecular beam epitaxy on Si(111) single crystal using an ultrathin high quality iron silicide as seed layer. STM analysis showed that the growth mode is of Volmer-Weber (island) type leading to a rather rough surface. Conventional MOKE, TIBIIST, and SQUID magnetometers have been used to investigate magnetic properties versus Fe thickness. The onset of ferromagnetism occurs in the vicinity of the Fe islands percolation threshold, i.e., for $t_{Fe} \sim 4.5$ ML. The Curie temperature increases continuously with Fe coverage, varying from 135 K for $t_{Fe}=4.7$ ML to 260 K for $t_{Fe}=7.3$ ML. A switching of the magnetic easy axis from out-of-plane toward in-plane is observed at $t_{Fe} \sim 7$ ML. For coverage above 8 ML, the films are very soft in-plane as expected and the magnetic anisotropy is the superposition of a small but well reproducible thickness dependent cubic sixth-order contribution and a tiny uniaxial component with random character. Specifically the uniaxial anisotropy (anisotropy field amplitude usually much less than 4 Oe) seems to be thickness-independent and not related to any crystallographic sample direction whereas the sixth-order cubic anisotropy easy axis rotates from $\langle 1\text{-}10 \rangle$ to $\langle 1\text{-}21 \rangle$ directions at a coverage of about 20 ML. At this thickness an extremely soft film can therefore be prepared. Finally, the present study shows that TIBIIST is a highly sensitive method to investigate quantitatively even extremely fine details of in-plane magnetic anisotropy in ultrathin films.

ACKNOWLEDGMENTS

The authors thank the Centre National de la Recherche Scientifique (CNRS) and the Région Alsace for financial support.

*Corresponding author. Email address: guillaume.garreau@uha.fr

[1] G. A. Prinz and J. J. Krebs, Appl. Phys. Lett. **39**, 397 (1981).
[2] G. W. Anderson, M. C. Hanf, and P. R. Norton, Phys. Rev. Lett. **74**, 2764 (1995).
[3] M. Zölfl, M. Brockmann, M. Köhler, S. Kreuzer, T. Schweinböck, S. Miethaner, F. Bensch, and G. Bayreuther, J. Magn. Magn. Mater. **175**, 16 (1997).
[4] E. M. Kneedler, B. T. Jonker, P. M. Thibado, R. J. Wagner, B. V. Shanabrook, and L. J. Whitman, Phys. Rev. B **56**, 8163 (1997).
[5] A. Filipe, A. Schuhl, and P. Galtier, Appl. Phys. Lett. **70**, 127 (1997).
[6] Y. B. Xu, E. T. M. Kernohan, D. J. Freeland, A. Ercole, M. Tselepi, and J. A. C. Bland, Phys. Rev. B **58**, 890 (1998).
[7] C. Lallaizon, B. Lépine, S. Abadou, A. Schussler, A. Quémerais, A. Guivarc'h, G. Jézéquel, S. Députier, and R. Guérin, Appl. Surf. Sci. **123/124**, 319 (1998).
[8] F. Bensch, G. Garreau, R. Moosbühler, G. Bayreuther, and E. Beaurepaire, J. Appl. Phys. **89**, 7133 (2001).
[9] O. Thomas, Q. Shen, P. Schieffer, N. Tournerie, and B. Lépine, Phys. Rev. Lett. **90**, 017205 (2003).
[10] B. T. Jonker, J. J. Krebs, G. A. Prinz, and S. B. Qadri, J. Cryst. Growth **81**, 524 (1987).
[11] E. Reiger, E. Reinwald, G. Garreau, M. Ernst, M. Zölfl, F. Bensch, S. Bauer, H. Preis, and G. Bayreuther, J. Appl. Phys. **87**, 5923 (2000).
[12] M. Marangolo, F. Gustavsson, M. Eddrief, Ph. Sainctavit, V. H. Etgens, V. Cros, F. Petroff, J. M. George, P. Bencok, and N. B. Brookes, Phys. Rev. Lett. **88**, 217202 (2002).
[13] Y. -T. Cheng, Y.-L. Chen, M. M. Karmarkar, and W.-L. Meng, Appl. Phys. Lett. **59**, 953 (1991).
[14] J. M. Gallego, J. M. Garcia, J. Alvarez, and R. Miranda, Phys. Rev. B **46**, 13 339 (1992); J. Alvarez, A. L. Vazquez de Parga, J. J. Hinarejos, J. de la Figuera, E. G. Michel, C. Ocal, and R. Miranda, Phys. Rev. B **47**, 16 048 (1993).

[15] S. M. Rezende, J. A. S. Moura, F. M. de Aguiar, and W. H. Schreiner, J. Magn. Magn. Mater. **140**, 663 (1995).
[16] Z. H. Nazir, C.-K. Lo, and M. Hardiman, J. Magn. Magn. Mater. **156**, 435 (1996).
[17] M. Fanciulli, S. Degroote, G. Weyer, and G. Langouche, Surf. Sci. **377-379**, 529 (1997).
[18] R. Kläsges, C. Carbone, W. Eberhardt, C. Pampuch, O. Rader, T. Kachel, and W. Gudat, Phys. Rev. B **56**, 10 801 (1997).
[19] S. Yaegashi, T. Kurihara, and K. Satoh, J. Appl. Phys. **81**, 6303 (1997).
[20] S. Foss, C. Merton, R. Proksch, G. Skidmore, J. Schmidt, E. D. Dahlberg, T. Pokhil, and Y.-T. Cheng, J. Magn. Magn. Mater. **190**, 60 (1998).
[21] M. Cougo dos Santos, J. Geshev, J. E. Schmidt, S. R. Teixeira, and L. G. Pereira, Phys. Rev. B **61**, 1311 (2000).
[22] P. Castrucci, R. Gunnella, R. Bernardini, P. Falcioni, and M. De Crescenzi, Phys. Rev. B **65**, 235435 (2002); G. Gubbiotti, G. Carlotti, F. D'Orazio, F. Lucari, R. Gunnella, and M. De Crescenzi, Surf. Sci. **454-456**, 891 (2000).
[23] S. M. Rezende, J. A. S. Moura, F. M. de Aguiar, and W. H. Schreiner, Phys. Rev. B **49**, 15 105 (1994).
[24] R. Naik, C. Kota, J. S. Payson, and G. L. Dunifer, Phys. Rev. B **48**, 1008 (1993).
[25] M. Eddrief, Y. Wang, V. H. Etgens, D. H. Mosca, J.-L. Maurice, J. M. George, A. Fert, and C. Bourgognon, Phys. Rev. B **63**, 094428 (2001).
[26] N. Mattoso, D. H. Mosca, W. H. Schreiner, I. Mazzaro, and S. R. Teixeira, Thin Solid Films **272**, 83 (1996).
[27] K. R. Heim, G. G. Hembree, and M. R. Scheinfein, J. Appl. Phys. **76**, 8105 (1994).
[28] F. Zavaliche, W. Wulfhekel, H. Xu, and J. Kirschner, J. Appl. Phys. **88**, 5289 (2000).
[29] K.-H. Park, J. S. Ha, and W. S. Yun, Surf. Sci. **492**, 34 (2001).
[30] P. Bertoncini, P. Wetzel, D. Berling, G. Gewinner, C. Ulhaq-Bouillet, and V. Pierron-Bohnes, Phys. Rev. B **60**, 11 123 (1999).
[31] S. Hajjar, G. Garreau, S. Pelletier, D. Bolmont, and C. Pirri, Phys. Rev. B **68**, 033302 (2003).
[32] M. Krause, F. Blobner, L. Hammer, K. Heinz, and U. Starke, Phys. Rev. B **68**, 125306 (2003).
[33] C. Liu, E. R. Moog, and S. D. Bader, Phys. Rev. Lett. **60**, 2422 (1988); C. Liu and S. D. Bader, Phys. Rev. B **41**, 553 (1990); Z. Q. Qiu, J. Pearson, and S. D. Bader, Phys. Rev. Lett. **70**, 1006 (1993).
[34] D. P. Pappas, K. P. Kämper, and H. Hopster, Phys. Rev. Lett. **64**, 3179 (1990).
[35] R. Allenspach and A. Bischof, Phys. Rev. Lett. **69**, 3385 (1992).
[36] F. Baudelet, M. T. Lin, W. Kuch, K. Meinel, B. Choi, C. M. Schneider, and J. Kirschner, Phys. Rev. B **51**, 12 563 (1995).
[37] P. Ohresser, J. Shen, J. Barthel, M. Zheng, Ch. V. Mohan, M. Klaua, and J. Kirschner, Phys. Rev. B **59**, 3696 (1999).
[38] C. Chappert, D. Renard, P. Beauvillain, J. P. Renard, and J. Seiden, J. Magn. Magn. Mater. **54-57**, 795 (1986).
[39] F. J. A. den Broeder, W. Hoving, and P. J. H. Bloemen, J. Magn. Magn. Mater. **93**, 562 (1991).
[40] B. N. Engel, C. D. England, R. A. Van Leeuwen, M. H. Wiedmann, and C. M. Falco, Phys. Rev. Lett. **67**, 1910 (1991).
[41] M. Kak, R. Stephan, A. Mehdaoui, D. Berling, D. Bolmont, G. Gewinner, and P. Wetzel, Surf. Sci. **566-568**, 278 (2004).
[42] S. Zabrocki (unpublished).
[43] J. A. Stroscio, D. T. Pierce, and R. A. Dragoset, Phys. Rev. Lett. **70**, 3615 (1993).
[44] C. Pirri, U. Kafader, G. Gewinner, and P. Wetzel, Solid State Commun. **89**, 313 (1994).
[45] The drastic decrease of the experimental $2p_{3/2}$ core line intensity compared to the simulated one, for polar angles above 45°, results essentially from the instrument response.
[46] We defined here the different MOKE geometries by considering the external magnetic field orientation and the light-scattering plane with respect to the sample plane. In polar geometry, the field is applied along the film normal. The field lies in the film plane and in the light-scattering plane in longitudinal geometry. Actually, the magnetization orientation does not necessarily follow the external field direction and, consequently, the Kerr signal contains different Kerr effects. Moreover, a misalignment up to 5° of the external field with respect to the film normal or film plane has to be considered with our 77–400 K operating MOKE setup, which enhances the mixing of polar and longitudinal Kerr effects of the Kerr signal, as illustrated in the discussion of the main text.
[47] R. Bergholz and U. Gradmann, J. Magn. Magn. Mater. **45**, 389 (1984).
[48] C. M. Schneider, P. Bressler, P. Schuster, J. Kirschner, J. J. de Miguel, and R. Miranda, Phys. Rev. Lett. **64**, 1059 (1990).
[49] C. A. Ballentine, R. L. Fink, J. Araya-Pochet, and J. L. Erskine, Phys. Rev. B **41**, 2631 (1990).
[50] Y. Li and K. Baberschke, Phys. Rev. Lett. **68**, 1208 (1992); M. Farle, K. Baberschke, U. Stetter, A. Aspelmeier, and F. Gerhardter, Phys. Rev. B **47**, 11 571 (1993); G. Garreau, M. Farle, E. Beaurepaire, and K. Baberschke, Phys. Rev. B **55**, 330 (1997); U. Bovensiepen, P. Poupopoulos, M. Farle, and K. Baberschke, Surf. Sci. **402-404**, 396 (1998).
[51] H. J. Elmers, J. Hauschild, H. Höche, U. Gradmann, H. Bethge, D. Heuer, and U. Köhler, Phys. Rev. Lett. **73**, 898 (1994); H. J. Elmers and J. Hauschild, Surf. Sci. **320**, 134 (1994).
[52] F. O. Schumann, S. Z. Wu, G. J. Mankey, and R. F. Willis, Phys. Rev. B **56**, 2668 (1997).
[53] M. Henkel, S. Andrieu, P. Bauer, and M. Piecuch, Phys. Rev. Lett. **80**, 4783 (1998).
[54] M. Gajdzik, T. Trappmann, C. Sürgers, and H. v. Löhneysen, Phys. Rev. B **57**, 3525 (1998).
[55] G. A. T. Allan, Phys. Rev. B **1**, 352 (1970).
[56] D. S. Ritchie and M. E. Fisher, Phys. Rev. B **7**, 480 (1973).
[57] R. Zhang and R. F. Willis, Phys. Rev. Lett. **86**, 2665 (2001).
[58] D. Berling, G. Gewinner, M. C. Hanf, K. Hricovini, S. Hong, B. Loegel, A. Mehdaoui, C. Pirri, M. H. Tuilier, and P. Wetzel, J. Magn. Magn. Mater. **191**, 331 (1999).
[59] J. Hauschild, U. Gradmann, and H. J. Elmers, Appl. Phys. Lett. **72**, 3211 (1998); N. Weber, K. Wagner, H. J. Elmers, J. Hauschild, and U. Gradmann, Phys. Rev. B **55**, 14 121 (1997).
[60] P. Escudier, Ann. Phys. (N.Y.) **9**, 125 (1975).
[61] P. Bertoncini, P. Wetzel, D. Berling, A. Mehdaoui, B. Loegel, G. Gewinner, R. Poinsot, and V. Pierron-Bohnes, J. Magn. Magn. Mater. **237**, 191 (2001).
[62] H. Fritzsche, J. Kohlhepp, H. J. Elmers, and U. Gradmann, Phys. Rev. B **49**, 15 665 (1994); H. Fritzsche, H. J. Elmers, and U. Gradmann, J. Magn. Magn. Mater. **135**, 343 (1994).
[63] M. Farle, B. Mirwald-Schulz, A. N. Anisimov, W. Platow, and K. Baberschke, Phys. Rev. B **55**, 3708 (1997); F. Gerhardter, Yi Li, and K. Baberschke, Phys. Rev. B **47**, 11 204 (1993).

[64] *Magnétisme: Matériaux et Applications, Collection Grenoble Sciences–EDP Sciences* (2000).
[65] S. Hajjar, Ph.D. thesis, University of Mulhouse, 2004.
[66] J. H. Wolfe, R. K. Kawakami, W. L. Ling, Z. Q. Qiu, R. Arias, and D. L. Mills, J. Magn. Magn. Mater. **232**, 36 (2001).
[67] G. Garreau, J. L. Bubendorff, S. Hajjar, D. Berling, S. Zabroki, A. Mehdaoui, R. Stephan, P. Wetzel, G. Gewinner, and C. Pirri, Phys. Status Solidi C **1**, 3726 (2004).